Supporting Information For Insights into Dioxygen Binding on Nonheme Metal Centers: An ab initio Multireference Electronic Structure Analysis

Peng Zhang[a,b], Way-Zen Lee[c,d], Shengfa Ye[a]*

[a]State Key Laboratory of Catalysis, Dalian Institute of Chemical Physics, Chinese Academy of Sciences, Dalian 116023, China

[b]University of Chinese Academy of Sciences, Beijing 100049, China

[c]Department of Chemistry, National Taiwan Normal University, Taipei 11677, Taiwan

[d]Department of Medicinal and Applied Chemistry, Kaohsiung Medical University, Kaohsiung 807, Taiwan

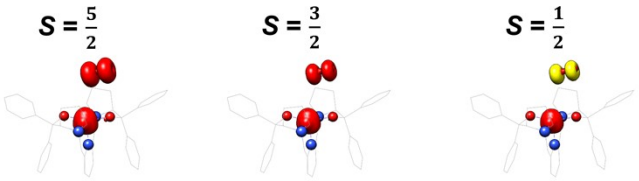

	Co: 2.85 (2.90) O_2: 1.99 (2.00)	Co: 2.09 (2.12) O_2: 0.80 (0.80)	Co: 1.58 (1.61) O_2: -0.66 (-0.66)
CAS(13,9) $d_{xz}d_{yz}d_{xy}d_{x^2-y^2}d_{z^2}\pi_{op}\pi_{ip}\pi^*_{op}\pi^*_{ip}$	88 % 221112211	87 % 221112211	87 % 221112211
CAS(15,10) $\sigma_{eq}d_{xz}d_{yz}d_{xy}d_{x^2-y^2}d_{z^2}\pi_{op}\pi_{ip}\pi^*_{op}\pi^*_{ip}$	88 % 2221112211	87 % 2221112211	86 % 2221112211
CAS(15,11) $d_{xz}d_{yz}d_{xy}d_{x^2-y^2}d_{z^2}\pi_{op}\pi_{ip}\pi^*_{op}\pi^*_{ip}\sigma\sigma^*$	88 % 22111221120	88 % 22111221120	87 % 22111221120
CAS(17,12) $\sigma_{eq}d_{xz}d_{yz}d_{xy}d_{x^2-y^2}d_{z^2}\pi_{op}\pi_{ip}\pi^*_{op}\pi^*_{ip}\sigma\sigma^*$	88 % 22111221120	87 % 22111221120	87 % 22111221120

Fig. S1. Spin populations on the Co center and the O_2 moiety, spin density and electron configurations for each spin state from CASSCF calculations with different choices of active spaces for complex Co(II)(BDPP) at the Co-O_2 bond length of 4.50 Å, only Co center and atoms of the first coordination-shell are shown for clarity.

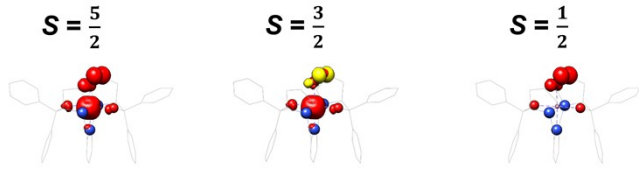

	Co: 3.66 (3.68) O_2: 1.03 (1.05)	Co: 3.28 (3.30) O_2: -0.52 (-0.54)	Co: 0.01 (0.00) O_2: 0.98 (0.99)
CAS(13,9) $d_{xz}d_{yz}d_{xy}d_{x^2-y^2}d_{z^2}\pi_{op}\pi_{ip}\pi^*_{op}\pi^*_{ip}$	100 % 221112211	95 % 221112211	95 % 221102212
CAS(15,10) $\sigma_{eq}d_{xz}d_{yz}d_{xy}d_{x^2-y^2}d_{z^2}\pi_{op}\pi_{ip}\pi^*_{op}\pi^*_{ip}$	99 % 2221112211	94 % 2221112211	93 % 2221102212
CAS(15,11) $d_{xz}d_{yz}d_{xy}d_{x^2-y^2}d_{z^2}\pi_{op}\pi_{ip}\pi^*_{op}\pi^*_{ip}\sigma\sigma^*$	96 % 22111221120	89 % 22111221120	91 % 22110221220
CAS(17,12) $\sigma_{eq}d_{xz}d_{yz}d_{xy}d_{x^2-y^2}d_{z^2}\pi_{op}\pi_{ip}\pi^*_{op}\pi^*_{ip}\sigma\sigma^*$	95 % 22111221120	87 % 22111221120	89 % 22110221220

Fig. S1. Spin populations on the Co center and the O_2 moiety, spin density and electron configurations for each spin state from CASSCF calculations with different choices of active spaces

for complex Co(II)(BDPP) at the Co-O_2 bond length of 1.91 Å, only Co center and atoms of the first coordination-shell are shown for clarity.

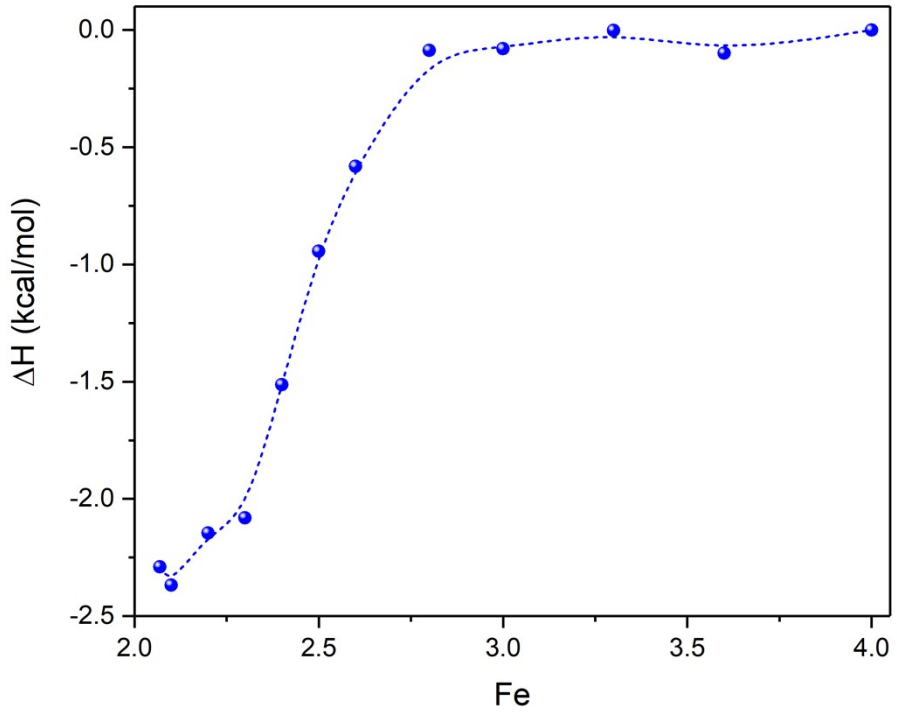

Fig. S3. DFT energy variation for the reaction of Fe(II)(BDPP) with O_2 on the septet potential energy surface as a function of the Fe–O_2 bond distance

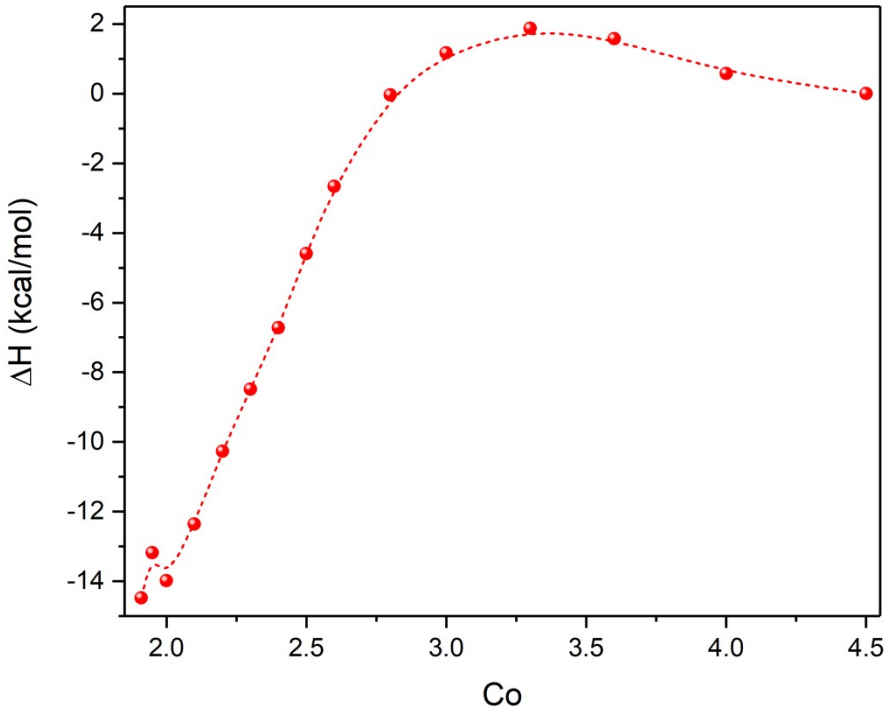

Fig. S4. DFT energy variation for the reaction of Co(II)(BDPP) with O_2 on the doublet potential energy surface as a function of the Co−O_2 bond distance

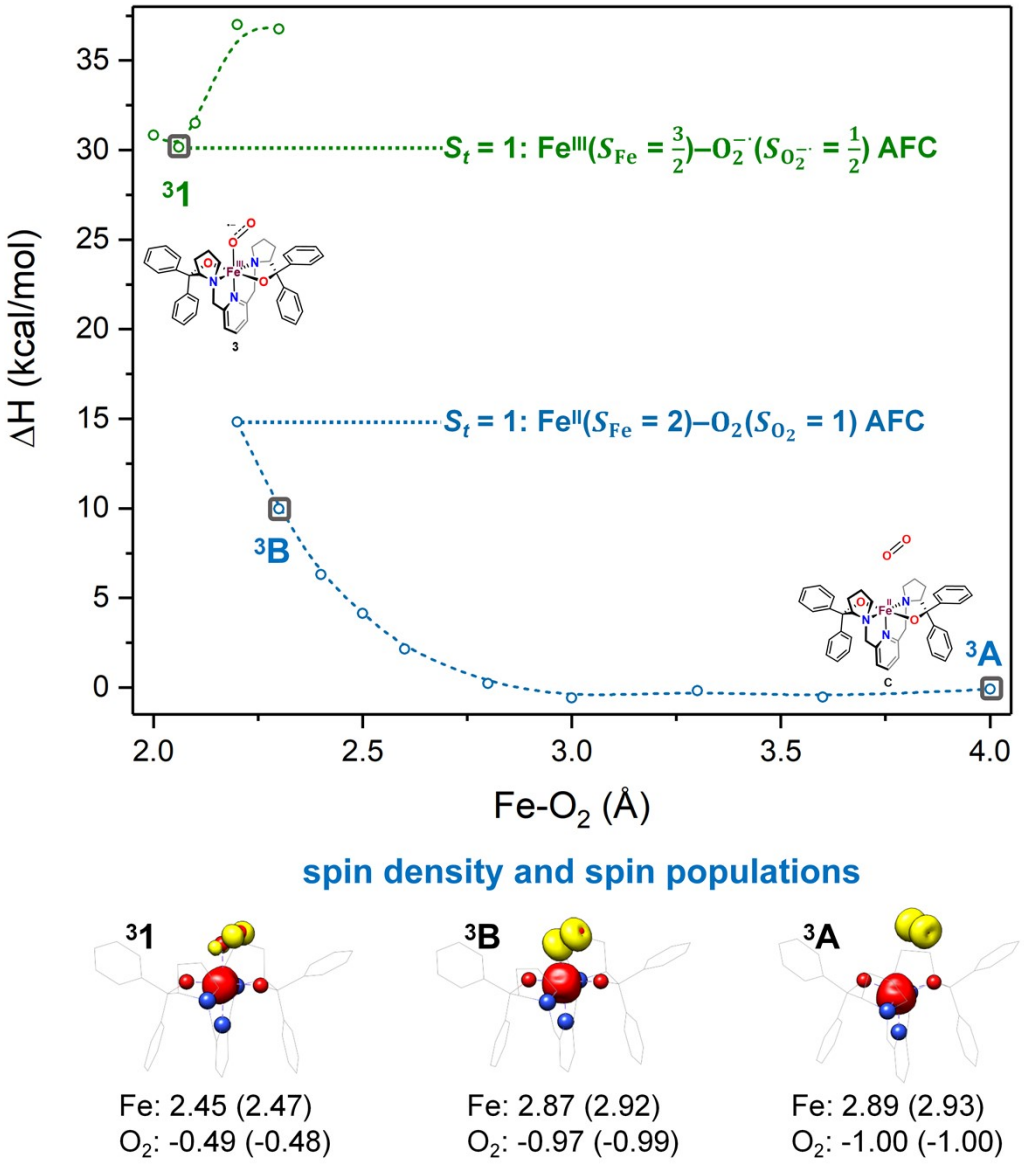

Fig. S5. (top) CASSCF(12,9)/NEVPT2 energy variation for the triplet reaction of Fe(II)(BDPP) with O_2 as a function of the Fe–O_2 bond distance; dot lines denote diabatic potential curves (azure line denotes an ^{S_t} = 1 Fe^{II}-O_2 complex, interpreted as an $^{S_{Fe}}$ = 2 Fe^{II} center antiferromagnetically coupled (AFC) with an $^{S_{O_2}}$ = 1 O_2 ligand; olive line denotes an ^{S_t} = 1 Fe^{III}-$O^{-\cdot}_2$ complex, interpreted as an $^{S_{Fe}} = \frac{3}{2}$ Fe^{III} center antiferromagnetically coupled (AFC) with an $^{S_{O^{-\cdot}_2}} = \frac{1}{2}$ $O^{-\cdot}_2$ ligand); (bottom) spin density and Löwdin spin populations on Fe center and O_2 unit calculated for complexes ^{3}**A** (Fe(II)(BDPP) + O_2), ^{3}**B**, and ^{3}**1** on the reaction trajectory are shown at the bottom and Mulliken spin populations featuring the same results are listed in parentheses, yellow and red denote negative and positive spin density, respectively, and local spin populations were also listed in **Table S4**; ligand atoms are omitted for clarity.

The binding of O_2 to Fe(II)(BDPP) on $S_t = 1$ potential surface also features two diabatic potential curves. One curve (azure line), described as a high spin Fe(II) center ($S_{Fe} = 2$) antiferromagnetically coupled with a triplet O_2 ligand ($S_{O_2} = 1$) (*vide infra*), rises in energy as the Fe-O_2 length declines from 4.00 Å to 2.20 Å, the other one (olive line), interpreted as a quartet Fe(III) center ($S_{Fe} = \frac{3}{2}$) antiferromagnetically coupled with a doublet superoxo ligand ($S_{O_2^{\cdot-}} = \frac{1}{2}$) (For more details, see below), decreases ranging from the Fe-O_2 length of 2.30 Å to 2.06 Å and increases for further reduction of the Fe-O_2 length, thus featuring a local minimal around 2.06 Å, which is 30.2 kcal/mol higher than complex ^{3}**A** in energy.

Complex ^{3}**A** with a Fe-O_2 bond length of 4.00 Å maintains a triplet ground state with a leading electron configuration of $d_{xz}^{\ 2}d_{yz}^{\ 1}d_{xy}^{\ 1}d_{x^2-y^2}^{\ 1}d_{z^2}^{\ 1}\pi_{ip}^{\ 2}\pi_{op}^{\ 2}\pi_{ip}^{*\ 1}\pi_{op}^{*\ 1}$ which occupies 94%. As demonstrated in **Fig. S5**, a double-layer donut-shaped spin density for the O_2 ligand and a nearly spherical spin density for the Fe(II) center suggest that spin populations are concentrated on a high spin Fe(II) center and π_{ip}^* and π_{op}^* MOs. Specifically, a high spin Fe(II) center is antiferromagnetically coupled to a triplet O_2 ligand. Therefore, following the same procedure, the electronic structure of complex ^{3}**A** could be evaluated as $|1,1\rangle = \sqrt{\frac{3}{5}}|2,-1\rangle - \sqrt{\frac{3}{10}}|1,0\rangle + \sqrt{\frac{1}{10}}|0,1\rangle$. This wavefunction yields the expectation values of S_z for Fe(II) center and O_2 ligand of $\frac{3}{2}$ and $-\frac{1}{2}$, respectively. The computed spin populations on Fe(II) center and O_2 ligand are 2.89 and -1.00, respectively, which are twice the expectation values of S_z for Fe(II) center and O_2 ligand, respectively, and confirm this wavefunction.

As depicted in **Fig. S5**, ^{3}**1** converges to a triplet state featuring noteworthy multireference character with a series of electron configurations of $d_{xz}^{\ 1}d_{yz}^{\ 1}d_{xy}^{\ 2}d_{x^2-y^2}^{\ 0}d_{z^2}^{\ 1}\pi_{ip}^{\ 2}\pi_{op}^{\ 2}\pi_{ip}^{*\ 2}\pi_{op}^{*\ 1}$ which account for 30%, $d_{xz}^{\ 2}d_{yz}^{\ 1}d_{xy}^{\ 2}d_{x^2-y^2}^{\ 0}d_{z^2}^{\ 1}\pi_{ip}^{\ 2}\pi_{op}^{\ 2}\pi_{ip}^{*\ 2}\pi_{op}^{*\ 0}$ which makes up 39%, and $d_{xz}^{\ 0}d_{yz}^{\ 1}d_{xy}^{\ 2}d_{x^2-y^2}^{\ 0}d_{z^2}^{\ 1}\pi_{ip}^{\ 2}\pi_{op}^{\ 2}\pi_{ip}^{*\ 2}\pi_{op}^{*\ 2}$ which occupies 27%. The last two terms show a remarkable chemical bonding interaction between d_{xz} and MO π_{op}^*. Again, the spin density on the O_2 ligand suggests negative spin is located on π_{op}^*, indicating the formation of a doublet superoxo ligand; the less spherical spin density for Fe(III) center compared to that for complex ^{7}**1**, indicates the formation of an intermediate spin Fe(III) center. As such, the electronic structure of complex ^{3}**1** could be evaluated as a quartet Fe(III) center ($S_{Fe} = \frac{3}{2}$) antiferromagnetically coupled with a

superoxo ligand ($S_{O_2^-} = \frac{1}{2}$) via a wavefunction of $|1,1\rangle = \sqrt{\frac{3}{4}}\left|\frac{3}{2}, -\frac{1}{2}\right\rangle - \sqrt{\frac{1}{4}}\left|\frac{1}{2}, \frac{1}{2}\right\rangle$ for complex ^{3}**1**. This wavefunction features the expectation values of S_z for Fe(III) center and O_2 ligand of $\frac{5}{4}$ and $-\frac{1}{4}$, respectively. The computed spin populations for Fe(III) center and O_2 ligand are 2.45 and -0.49, respectively, indicating that the coupling wavefunction is appropriate for interpreting the electronic structure of complex ^{3}**1**.

For the O_2 ligand binding to Fe(II)(BDPP), as the Fe-O_2 distance decreases from 4.00 Å to 2.20 Å (azure line), the wavefunction shows strong multireference character with a series of electron configurations of $d_{xz}^{\ 2}d_{yz}^{\ 1}d_{xy}^{\ 1}d_{x^2-y^2}^{\ 1}d_{z^2}^{\ 1}\pi_{ip}^{\ 2}\pi_{op}^{\ 2}\pi_{ip}^{*\,1}\pi_{op}^{*\,1}$, $d_{xz}^{\ 2}d_{yz}^{\ 1}d_{xy}^{\ 1}d_{x^2-y^2}^{\ 1}d_{z^2}^{\ 1}\pi_{ip}^{\ 2}\pi_{op}^{\ 2}\pi_{ip}^{*\,2}\pi_{op}^{*\,1}$, and $d_{xz}^{\ 2}d_{yz}^{\ 1}d_{xy}^{\ 1}d_{x^2-y^2}^{\ 2}d_{z^2}^{\ 1}\pi_{ip}^{\ 2}\pi_{op}^{\ 2}\pi_{ip}^{*\,0}\pi_{op}^{*\,1}$. The last two terms show significant chemical bonding interaction between π_{ip}^{*} and $d_{x^2-y^2}$. During this process, the weights of the last two increase (0%→33% and 0%→17%) and the weight of the first one decreases (94%→37%). Starting from the Fe-O_2 bond length of 2.30 Å (olive line), the wavefunction remains the same as that of complex ^{3}**1**. To accomplish the transformation of complex ^{3}**A** to complex ^{3}**1**, an electron is shifted from the Fe(II) center to the O_2 ligand concurrent with an electronic-structure rearrangement of the Fe(III) center.

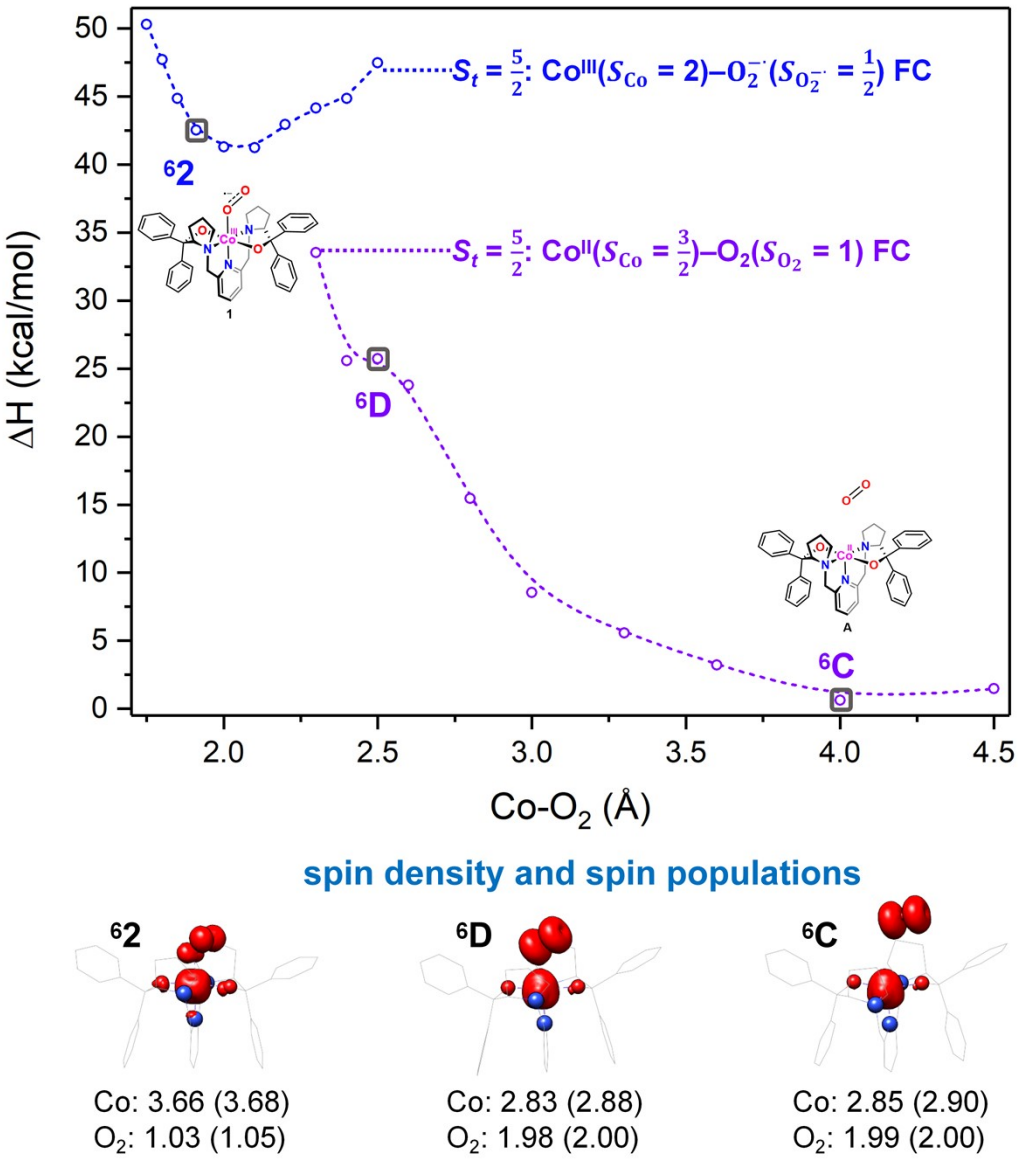

Fig. S6. (top) CASSCF(13,9)/NEVPT2 energy variation for the reaction of Co(II)(BDPP) with O_2 as a function of the Co–O_2 bond distance; dot lines denote diabatic potential curves (violet line denotes an $S_t = \frac{5}{2}$ Co^{II}-O_2 complex, interpreted as an $S_{Co} = \frac{3}{2}$ Co^{II} center ferromagnetically coupled (FC) with an $S_{O_2} = 1$ O_2 ligand; blue line denotes an $S_t = \frac{5}{2}$ Co^{III}-$O_2^{-\cdot}$ complex, interpreted as an $S_{Co} = 2$ Co^{III} center ferromagnetically coupled (FC) with an $S_{O_2^{-\cdot}} = \frac{1}{2}$ $O_2^{-\cdot}$ ligand); (bottom) spin density and Löwdin spin populations on Fe center and O_2 unit calculated for complexes ^{6}**C** (Co(II)(BDPP) + O_2), ^{6}**D**, and ^{6}**2** on the reaction trajectory are shown at the bottom and Mulliken spin populations featuring the same results are listed in parentheses, yellow and red denote negative and positive spin density, respectively, and local spin populations were also listed in **Table S5**; ligand atoms are omitted for clarity.

Depicted in **Fig. S6** is CASSCF(13,9) potential energy surface of O_2 binding on complex Co(II)(BDPP) in $S_t = \frac{5}{2}$ state. Starting points ^{6}**C** having a Co-O_2 distance of 4.00 Å features a leading electron configuration of $d_{xz}^2 d_{yz}^2 d_{xy}^1 d_{x^2-y^2}^1 d_{z^2}^1 \pi_{ip}^2 \pi_{op}^2 \pi_{ip}^{*1} \pi_{op}^{*1}$ accounting for 87% of the wavefunction. Therefore, its electronic structure is best characterized as a high spin Co(II) center ($S_{Co} = \frac{3}{2}$) ferromagnetically coupled to a triplet O_2 ligand ($S_{O_2} = 1$) affording an overall $S_t = \frac{5}{2}$ state, in line with the computed spin density shown in **Fig. S6**. Furthermore, the estimated spin populations on the Co(II) center and the O_2 unit being 2.85 and 1.99, respectively, confirm this electronic-structure description. And complex ^{6}**2** also maintains a sole electron configuration of $d_{xz}^2 d_{yz}^1 d_{xy}^1 d_{x^2-y^2}^1 d_{z^2}^1 \pi_{ip}^2 \pi_{op}^2 \pi_{ip}^{*2} \pi_{op}^{*1}$ (100%) interpreted as a high spin Co(III) center ferromagnetically coupled to a doublet $O_2^{-\cdot}$ ligand ($S_{O_2^{-\cdot}} = \frac{1}{2}$) which is also confirmed by the computed spin populations on Fe(III) center and O_2 ligand (3.66 for Fe(III) center and 1.03 for $O_2^{-\cdot}$ ligand). Furthermore, complex ^{6}**2** is 41.2 kcal/mol higher than complex ^{6}**C** in energy.

For the O_2 binding process to afford ^{6}**2**, as the Co-O_2 distance contracts from 4.00 Å to 2.30 Å (violet curve), the weight of the main electron configuration of $d_{xz}^2 d_{yz}^2 d_{xy}^1 d_{x^2-y^2}^1 d_{z^2}^1 \pi_{ip}^2 \pi_{op}^2 \pi_{ip}^{*1} \pi_{op}^{*1}$ keeps constant and no multireference character is observed. Moreover, the spin density and spin populations computed for ^{6}**D** are nearly identical to those for ^{6}**C**, demonstrating that the electronic structure of ^{6}**D** is nearly identical to that of ^{6}**C**. Comparison of the electronic structures of complexes ^{6}**C** and ^{6}**2** suggests that, as the Co-O_2 bond length further descends, one β electron in the Co d_{yz} orbital migrates into O_2 π_{ip}^* to furnish ^{6}**2**.

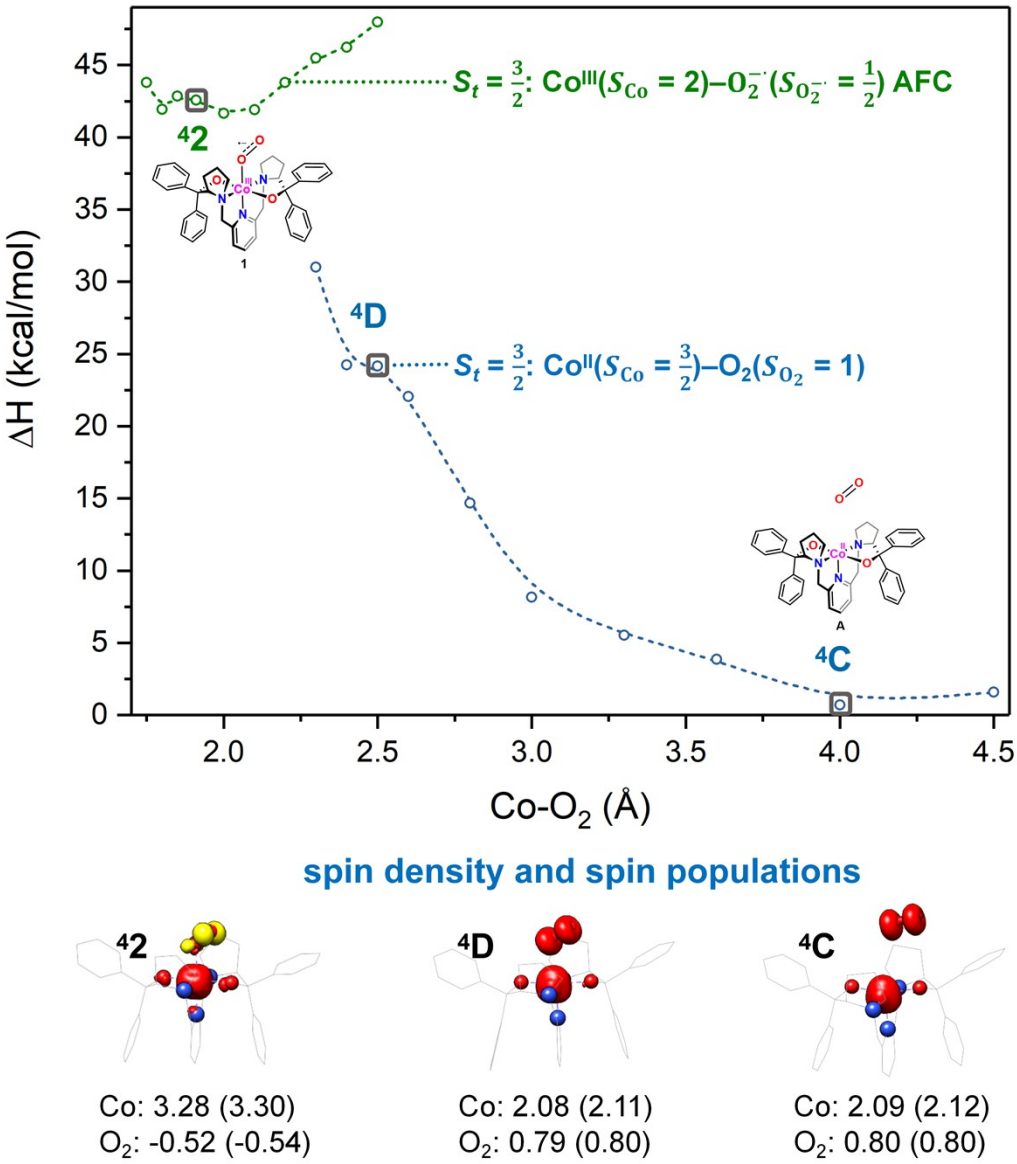

Fig. S7. CASSCF(13,9)/NEVPT2 energy variation for the binding of O_2 to Co(II)(BDPP) on $^{S_t = \frac{3}{2}}$ potential surface as a function of the Co−O_2 bond distance; dot lines donate diabatic potential curves (azure line donates a quartet Co^{II}-O_2 complex, interpreted as a quartet Co^{II} ferrimagnetically coupled with a triplet O_2 ligand; olive line donates a quartet Co^{III}-$O_2^{\bullet-}$ complex, interpreted as a quartet Co^{III} antiferromagnetically coupled (AFC) with a doublet $O_2^{\bullet-}$ ligand); (bottom) spin density and Löwdin spin populations on Fe center and O_2 unit calculated for complexes ^{4}**C** (Co(II)(BDPP) + O_2), ^{4}**D**, and ^{4}**2** on the reaction trajectory are shown at the bottom and Mulliken spin populations featuring the same results are listed in parentheses, yellow and red denote negative and positive spin density, respectively, and local spin populations were also listed in **Table S5**; ligand atoms are omitted for clarity.

As demonstrated in **Fig. S7**, the reaction of O_2 with Co(II)(BDPP) on $S_t = \frac{3}{2}$ potential surface also maintains two diabatic $S_t = \frac{3}{2}$ potential curves, whereas the azure line donates a quartet Co(II) compound magnetically coupled to a triplet O_2 ligand to yield an overall $S_t = \frac{3}{2}$ ground state (see below for details), and the olive line represents a quintet Co(III) compound antiferromagnetically coupled with a doublet superoxo ligand (*vide infra*). The azure line is energetically uphill as the Co-O_2 distance declines from 4.00 Å to 2.30 Å, while the olive line initially decreases in energy ranging from the Co-O_2 distance of 2.50 Å to 2.00 Å, and rises again for further reduction of the Co-O_2 distance, thereby affording a local minimal around the Co-O_2 distance of 2.00 Å, which is 41.7 kcal/mol higher than reactant complex ^{4}C in energy.

Reactant complex ^{4}**C** with a Co-O_2 bond length of 4.00 Å, features a quartet ground state with a leading electron configuration of $d_{xz}^{\ 2}d_{yz}^{\ 2}d_{xy}^{\ 1}d_{x^2-y^2}^{\ 1}d_{z^2}^{\ 1}\pi_{ip}^{\ 2}\pi_{op}^{\ 2}\pi_{ip}^{*\ 1}\pi_{op}^{*\ 1}$ which makes up 82%. Following the same procedure, as depicted in **Fig. S7**, the spin density for complex ^{4}**C** is similar to that for complex ^{6}**C** but features a smaller size, which suggests a high spin Co(II) compound magnetically coupled with a triplet O_2 ligand to yield an overall $S_t = \frac{3}{2}$ ground state. Thus, following the same procedure, this quartet state could be described by $\left|\frac{3}{2},\frac{3}{2}\right\rangle = \sqrt{\frac{3}{5}}\left|\frac{3}{2},0\right\rangle - \sqrt{\frac{2}{5}}\left|\frac{1}{2},1\right\rangle$ which gives the expectation values of S_z of $\frac{11}{10}$ and $\frac{2}{5}$ for the Co(II) center and the O_2 ligand, respectively. Thus, the computed spin populations confirm that this wavefunction could accurately describe the electronic structure of complex ^{4}**C**.

As shown in **Fig. S7**, the spin density on the O_2 ligand for complex ^{4}**2** indicates negative spin is located on π_{op}^{*}, while the more spherical spin density located on Co center compared to those for complexes ^{4}**C** and ^{4}**D**, suggests a high spin Co(III) center for complex ^{4}**2**. As such, complex ^{4}**2** is better described as a high spin Co(III) center antiferromagnetically coupled with a superoxo ligand, which could be evaluated as $\left|\frac{3}{2},\frac{3}{2}\right\rangle = \sqrt{\frac{4}{5}}\left|2,-\frac{1}{2}\right\rangle - \sqrt{\frac{1}{5}}\left|1,\frac{1}{2}\right\rangle$. This wavefunction yields the expectation values of S_z of $\frac{9}{5}$ and $-\frac{3}{10}$ for a high spin Co(III) center and a superoxo ligand, respectively. The computed spin populations of a high spin Co(II) center and a superoxo ligand (3.28 for high spin Co(III) center and -0.52 for superoxo ligand) are in line with the theoretical analyses, indicating that this wavefunction is suitable for describing the electronic structure of complex ^{4}**2**.

Regarding the binding process, as O_2 approaches Co(II)(BDPP) from 4.00 Å to 2.30 Å (azure line), the wavefunction exhibits multireference character, whereas the wavefunction of complex ^{4}**D** could be evaluated by a series of electron configurations of $d_{xz}^{\ 2}d_{yz}^{\ 2}d_{xy}^{\ 1}d_{x^2-y^2}^{\ 1}d_{z^2}^{\ 1}\pi_{ip}^{\ 2}\pi_{op}^{\ 2}\pi_{ip}^{*\ 1}\pi_{op}^{*\ 1}$

which accounts for 32%, $d_{xz}^{2}d_{yz}^{2}d_{xy}^{1}d_{x^2-y^2}^{1}d_{z^2}^{0}\pi_{ip}^{2}\pi_{op}^{2}\pi_{ip}^{*2}\pi_{op}^{*1}$ which makes up 32%, and $d_{xz}^{2}d_{yz}^{2}d_{xy}^{1}d_{x^2-y^2}^{1}d_{z^2}^{2}\pi_{ip}^{2}\pi_{op}^{2}\pi_{ip}^{*0}\pi_{op}^{*1}$ which occupies 16%. The last two configurations demonstrate strong chemical bonding interaction between π_{ip}^{*} and d_{z^2} MOs. Spin density for complex ^{4}**D**, which is similar to that for complex ^{4}C, suggests the shift of positive spin on π_{ip}^{*} to π_{op}^{*}, indicating the preparation for electron transfer from the Co(II) center to the O_2 ligand. Starting from the Co-O_2 distance of 2.50 Å, ^{4}**2** could converge to another quartet wavefunction (olive line) with a leading electron configuration of $d_{xz}^{2}d_{yz}^{1}d_{xy}^{1}d_{x^2-y^2}^{1}d_{z^2}^{1}\pi_{ip}^{2}\pi_{op}^{2}\pi_{ip}^{*2}\pi_{op}^{*1}$ which accounts for 95%. To finish the conversion of complexes ^{4}**C** to ^{4}**2**, one electron is shifted from the Co(II) center to the O_2 ligand in combination with a fast reorganization of the electronic structure of the Co(III) center.

Table S1. Configuration and weights for complex **2** at the Co-O_2 bond length of 1.91 Å with distinct basis sets from CASSCF(13,9)/NEVPT2 calculations.

	configuration	def2-SV	def2-SVP	def2-TZVP	def2-TZVPP
doublet	222222100	0.94339	0.94662	0.94776	0.94806
quartet	222211111	0.93259	0.94809	0.95315	0.95391
sextuplet	222211111	0.99084	0.94809	0.99600	0.99660

Table S2. Configuration and weights for complex **2** at the Co-O_2 bond length of 4.50 Å with distinct basis sets from CASSCF(13,9)/NEVPT2 calculations.

	configuration	def2-SV	def2-SVP	def2-TZVP	def2-TZVPP
doublet	222222100	0.86253	0.87038	0.86511	0.85727
quartet	222211111	0.86430	0.87296	0.87059	0.86718
sextet	222211111	0.86721	0.87729	0.87968	0.88363

Table S3. Configuration and weights for complex **2** at the Co-O_2 bond length of 2.50 Å with distinct basis sets from CASSCF(13,9)/NEVPT2 calculations.

	configuration	def2-SV	def2-SVP	def2-TZVP	def2-TZVPP
doublet	222222100	0.86253	0.87038	0.86511	0.85727
quartet	222211111	0.86430	0.87296	0.87059	0.86718
sextet	222211111	0.86721	0.87729	0.87968	0.88363

Table S4. Local spin populations for Fe center and O_2 ligand from CASSCF(12,9)/NEVPT2 calculations.

	^{3}A	^{3}B	^{3}**1**	^{5}A	^{5}B	^{5}**1**	^{7}A	^{7}B	^{7}**1**
Fe	2.79	2.76	2.37	3.10	3.09	4.30	3.72	3.73	4.62

O_2	-0.98	-0.93	-0.46	0.66	0.65	-0.59	1.97	1.93	0.99

Table S5. Local spin populations for Co center and O_2 ligand from CASSCF(13,9)/NEVPT2 calculations.

	^{2}C	^{2}D	^{2}**2**	^{4}C	^{4}D	^{4}**2**	^{6}C	^{6}D	^{6}**2**
Co	1.56	1.52	0.01	2.03	2.02	3.23	2.77	2.76	3.60
O_2	-0.66	-0.62	0.92	0.79	0.76	-0.50	1.97	1.91	0.97

Table S6. Löwdin spin populations for Fe center and O_2 ligand from DFT calculations.

	^{3}A	^{3}B	^{3}**1**	^{5}A	^{5}B	^{5}**1**	^{7}A	^{7}B	^{7}**1**
Fe	3.62	3.24	3.08	1.90	3.20	4.09	3.62	4.01	4.10
O_2	-1.99	-1.50	-1.31	1.99	0.56	-0.78	2.00	1.33	1.20

Table S7. Mulliken spin populations for Fe center and O_2 ligand from DFT calculations.

	^{3}A	^{3}B	^{3}**1**	^{5}A	^{5}B	^{5}**1**	^{7}A	^{7}B	^{7}**1**
Fe	3.71	3.34	3.18	1.93	3.29	4.15	3.71	4.08	4.16
O_2	-2.00	-1.52	-1.33	2.00	0.55	-0.79	2.00	1.33	1.20

Table S8. Löwdin spin populations for Co center and O_2 ligand from DFT calculations.

	^{2}C	^{2}D	^{2}**2**	^{4}C	^{4}D	^{4}**2**	^{6}C	^{6}D	^{6}**2**
Co	2.59	1.67	-0.02	0.93	1.61	1.82	2.59	2.83	3.03
O_2	-1.99	-0.80	1.00	1.99	1.16	0.85	1.99	1.46	1.13

Table S9. Mulliken spin populations for Co center and O_2 ligand from DFT calculations.

	^{2}C	^{2}D	^{2}**2**	^{4}C	^{4}D	^{4}**2**	^{6}C	^{6}D	^{6}**2**
Co	2.62	1.69	-0.03	0.94	1.63	1.84	2.62	2.83	3.00
O_2	-1.99	-0.90	1.01	1.99	1.18	0.85	1.99	1.46	1.14

Table S10. Energy variations for the reaction of O_2 with complex Co(II)(BDPP) from CASSCF and CASSCF/NEVPT2 calculations (kcal/mol).

Co-O (Å)	$S=\frac{1}{2}$		$S=\frac{3}{2}$		$S=\frac{5}{2}$	
	CASSCF	NEVPT2	CASSCF	NEVPT2	CASSCF	NEVPT2
1.8	84.0	9.6	75.6	42.2	78.7	49.3
1.8	82.0	7.5	73.0	40.4	75.4	46.1
1.9	81.1	5.9	71.7	41.4	72.4	43.3
1.9	81.5	5.8	70.5	41.2	70.3	40.9
2.0	83.6	7.7	70.0	40.4	69.6	39.7
2.1	87.2	10.0	71.5	40.5	71.1	39.7
2.2	91.5	14.2	73.8	42.3	73.5	41.6
2.3	55.0	18.2	55.8	30.1	57.6	33.3
2.4	42.5	22.2	43.0	23.2	44.2	25.3
2.5	42.9	22.6	43.3	23.4	44.2	24.9

2.6	40.6	21.4	41.0	22.0	41.6	23.1
2.8	28.5	14.2	28.6	14.5	28.9	15.0
3.0	16.4	7.7	16.5	7.9	16.7	8.1
3.3	9.0	4.3	9.0	4.3	9.1	4.4
3.6	5.0	2.7	5.1	2.8	5.1	2.8
4.0	0.0	0.0	0.0	0.0	0.0	0.0
4.5	1.1	0.4	1.1	0.4	1.1	0.4

Table S11. Table S3. Energy variations for the reaction of O_2 with complex Fe(II)(BDPP) from CASSCF and CASSCF/NEVPT2 calculations (kcal/mol).

Fe-O (Å)	*S* = 1		*S* = 2		*S* = 3	
	CASSCF	NEVPT2	CASSCF	NEVPT2	CASSCF	NEVPT2
2.0	77.0	29.6	20.0	6.3	21.2	8.8
2.1	79.3	28.9	21.3	4.8	22.2	6.9
2.1	80.6	30.3	22.2	5.8	23.0	7.5
2.2	31.8	13.6	26.2	10.6	26.7	11.7
2.3	26.5	10.4	27.0	11.4	28.2	12.8
2.4	20.9	7.5	21.3	8.2	22.0	9.4
2.5	16.0	5.0	16.2	5.4	16.7	6.1
2.6	12.0	2.6	12.2	2.9	12.5	3.3
2.8	6.7	0.6	6.8	0.7	6.9	0.9
3.0	3.9	-0.4	4.0	-0.3	4.0	-0.2
3.3	1.6	-0.7	1.6	-0.7	1.6	-0.6
3.6	0.7	-0.4	0.7	-0.4	0.7	-0.4
4.0	0.0	0.0	0.0	0.0	0.0	0.0